American Journal of Mathematical and Computational Sciences
2017; 2(5): 30-38
http://www.aascit.org/journal/ajmcs

AASCIT American Association for Science and Technology

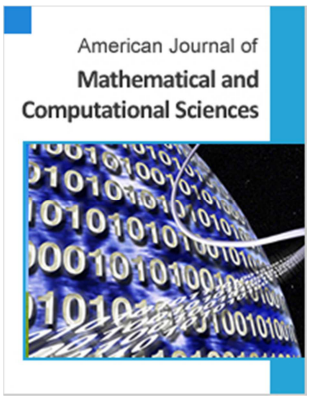

Keywords
Merging of Medical Images,
Counterlet Transform,
Multi-modality,
Multi-fractal Spectrum,
Human Vision and
Comprehension

Received: June 11, 2017
Accepted: August 6, 2017
Published: September 14, 2017

Medical Image Fusion in Transformation Domain Using Smart Methods

Reza Takht Kinai, Yousef Farhang

Department of Computer Sciences, Khoy Branch, Islamic Azad University, Khoy, Iran

Email address

rezatakhtkiani@gmail.com (R. T. Kinai), yfarhang@yahoo.com (Y. Farhang)

Citation

Reza Takht Kinai, Yousef Farhang. Medical Image Fusion in Transformation Domain Using Smart Methods. *American Journal of Mathematical and Computational Sciences.* Vol. 2, No. 5, 2017, pp. 30-38.

Abstract

Multimodality merging of medical images has developed as a powerful tool for clinical applications by the rise of different modalities of medical images. The main incentive was to obtain relevant information from different sources as a single output which plays a key role in medical diagnosis. A good image fusion algorithm should preserve all significant features of the source image and provide as few contradictions in the results as possible. Contourlet can provide less heterogeneity in multi-resolution and directional and positional properties of 2D signals compared to other image opening methods. In this work it was tried to develop an algorithm for medical image fusion by combining contourlet transformation and multi-fractal spectrum in which the fused image can provide more information for each of the input sources of the merged image resulting in more suitable images for human vision and comprehension and clinical applications. The efficiency is shown using different tests on different medical images. In addition, improved performance of the proposed framework compared to other methods was observed.

1. Introduction

Medical imaging includes some imaging techniques capable of being used as noninvasive methods to see the inside of the body. This means that physicians do not need surgery to see the inside of the body. These types of imaging are used to help the diagnosis or treatment in different medical conditions. Imaging techniques use radiation or a spectrum of electromagnetic waves for imaging. This technique may provide scans with complementary and sometimes contradictory information. Often a combination of images result in added clinical information in separate images. When there is the possibility of creating images by different methods, combining the images would also be possible; for example, the combination of an anatomical image such as CT or MRI with a functional image such as PET, SPECT or FMRI when they are balanced or are imaged simultaneously. In a functional image, for example, often anatomic details are not enough for positioning a damage or tumor [1]. Through fast and increasing growth in medical imaging equipment, this technology has become a critical part of applied programs including diagnosis, examination and treatment. These advancements has made it possible for the radiologists to quickly obtain more realistic and efficient images from internal organs of the body. These images are often in the form of medical modality images such as X-ray, computerized tomography (CT), magnetic resonance imaging (MRI), magnetic resonance angiography (MRA) and positron emission tomography (PET). This modality of medical images generally provides complementary and sometimes contradictory medical information. For example, X-ray and CT images can

provide images of dense structures such as bones and implants with lower noise but cannot recognize physiologic changes. Similarly, normal and pathologic tissues can be better shown in MRI images while PET images provide better information on blood flow with lower resolution. For medical diagnosis and treatment planning and evaluation, complementary information obtained from images taken with differentmethods are required. For example, a combination of simultaneous PET/CT imaging can be used to reveal anatomic and physical features of human body and also to monitor tumor activities and anatomic sources of cancer. Also, in the diagnosis of body organs in which the detection of tumor boundaries are difficult, PET/CT imaging can be useful. Therefore, combination of multi-modality medical images is necessary and is currently a very promising research field. Image fusion can be important as a procedure in which some important features of the images can be obtained from different inputs and their transformation to a single image without loss of information in order to integrate complementary information obtained from images with different modalities to get more complete and precise information from similar objects [2-3].

2. The Proposed Technique

A good image fusion algorithm should preserve all significant properties in the source images and provide as few contradictions in the results as possible. Contourlet can provide less heterogeneity in multi-resolution and directional and positional properties of 2D signals compared to other image opening methods. In this work it was tried to develop an algorithm for medical image fusion by combining contourlet transformation and multi-fractal spectrum in which the fused image can provide more information for each of the input sources of the merged image resulting in more suitable images for human vision and comprehension and clinical applications.

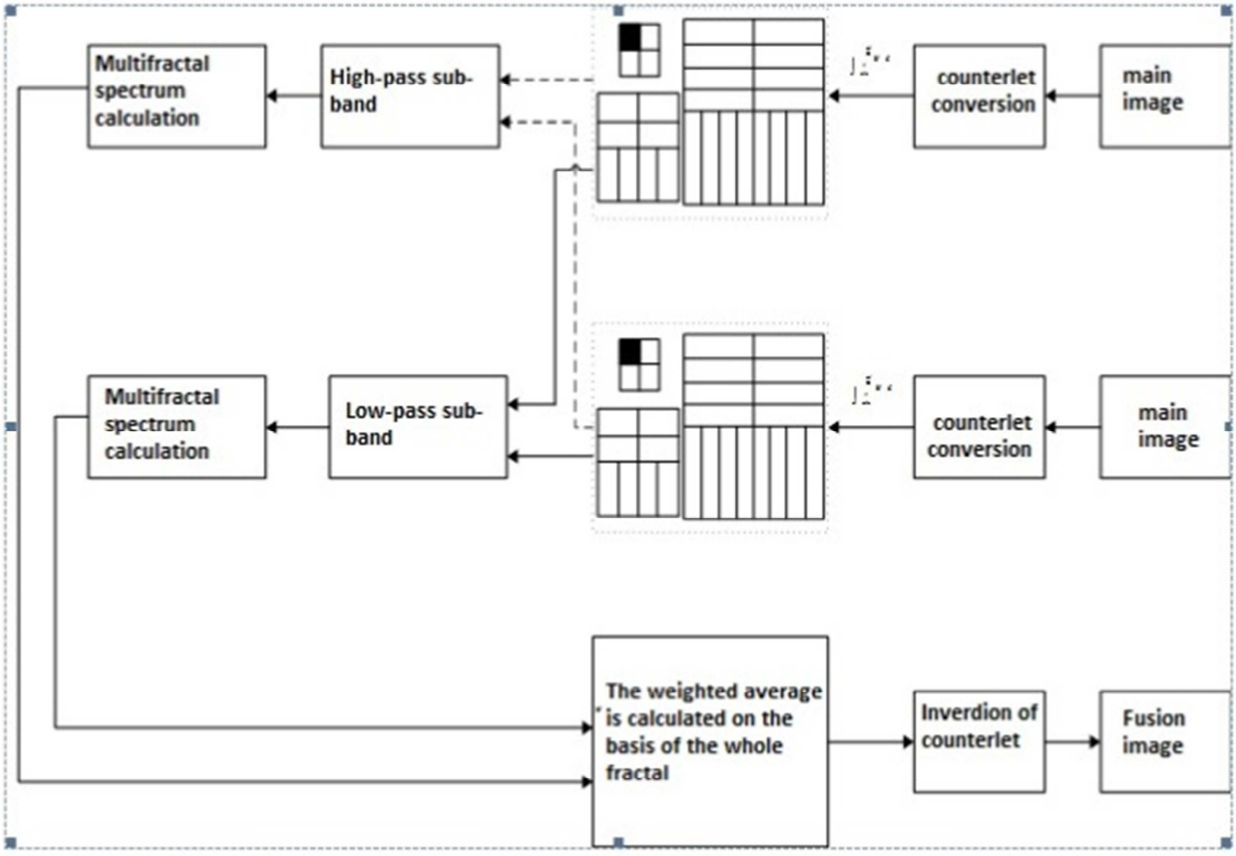

Figure 1. *Block diagram of image fusion based on counterlet and multi-fractal spectrum.*

General principle of fusion algorithm based on counterlet and multi-fractal spectrum is shown in Figure 1. This figure shows the input sources for the creation of fused image. Each of the blocks in Figure 1 are decomposed by counterlet conversion. After counterlet decomposition, the input image is decomposed into several low-pass and high-pass sub-bands in different directions and scales. Each of the low-pass and high-pass sub-band shows high-frequency details in different directions and scales. After decomposition into low-pass and high-pass sub-bands, multi-fractal spectrum is calculated for each sub-band and then weight average of these fractal spectra is obtained and finally counterlet conversion is inverted to create fused image.

$$Weighted\ Mean = \frac{(FD_{(i)} \times C_i) + (FD_{(j)} \times C_j)}{(FD_{(i)} + FD_{(j)})}$$

For color images, figure 1 is repeated for each RGB channel.

3. Test Results

In medical diagnoses, novel imaging techniques such as computerized tomography (CT), ultrasound, PET, NMR, etc. help physicians find the position of abnormal masses examine anatomical organs. Each of these imaging techniques have their own advantages and disadvantages. For example, a good view of bones and other dense structures can be obtained in CT images. Under special conditions, soft and dense tissues have to be images to provide a better diagnosis. Therefore, there is a need for fusion of different types of images for better treatment.

An information source for imaging system is a center which performs compilation of clinical information from MR and CT images as well as nuclear medical images. ATLAS project was collected by neurology radiology department of Brigham and Women's Hospital of Harvard Medical University, Countway medical library and American Academy of Neurology [11].

Datasets were consisted of 256×256 images which were downloaded from the brain of Harvard Medical University's website at http://www.med.harvard.edu/aanlib/home.html. The above atlas can be considered as an introduction to neuroanatomy by emphasizing on human brain anatomy and human neurological system diseases were investigated. This website tries to show a wide range of human brain diseases ad anomalies. The website contains examples of human brain diseases which can be shown with a combination of different images and imaging frequencies. Nothing in this website is considered as medical advice. The images in this website are all high quality images from inside human head. The images are visual results of human brain diseases such as stroke, Alzheimer's disease and even diseases such as mad cow. Harvard Medical University's ATLAS and medical image catalogue of this website are real human brain images which were taken from natural and healthy as well as diseased, injured and irregular tissues; a collection of 100 different structures in the brain with consistent performance and anatomy of healthy human brain.

The test data in this work consisted of a collection of brain images which are briefly described here.

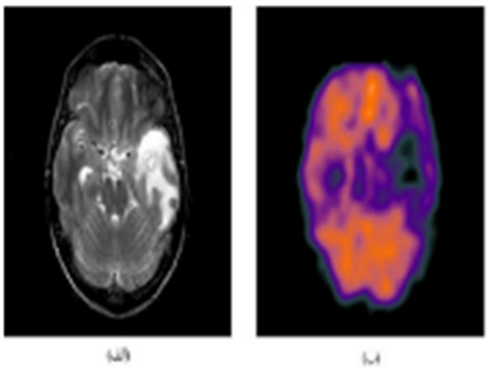

A

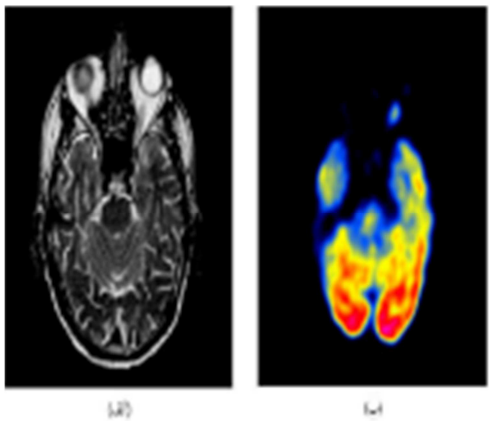

B

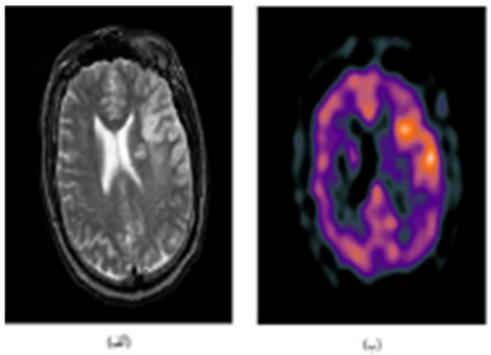

C

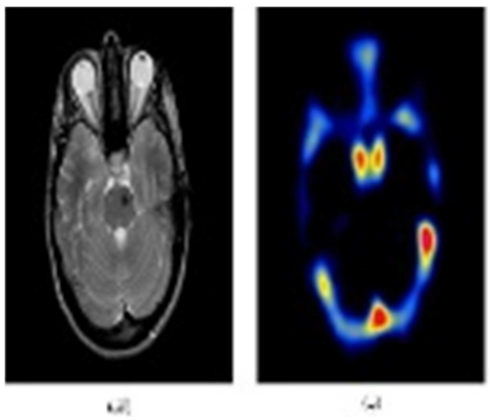

D

Figure 2. *(A): brain images of a 42-year old woman; a) MRI image, b) SPECT image. Figure A belongs to a 42-year old woman with long history of tobacco consumption. One month before the image was taken this woman had severe headache. (B): brain images of a 48-year old man; a) MRI image, b) SPECT image. Figure belongs to a 48-year old right-handed man who experiences speaking difficulties in the workplace. (C): brain images of a 70-year old man; a) MRI image, b) SPECT image. Figure C belongs to a 70-year old man who experienced memory problems 9 months before the image was taken. (D): brain images of a 26-year old woman; a) MRI image, b) SPECT image. Figure belongs to a 26-year old woman with 10 years of headache history which had recently experienced pain attack to right knee and reduction of leg performance following a surgery.*

Statistical analysis of different fusion techniques along with visual evaluation is very important due to extensive use of multispectral images in medical diagnosis. Therefore powerful evaluation tools for the comparison of the results

obtained from different techniques is needed. Generally a complete fused image is unknown and obtaining its results is difficult. This has resulted in the inability of the fused images compared to the standard. For human observations the performance of fusion algorithm can be described as the improvement of the user performance in tasks such as identification, diagnosis or classification. These are all based on physical visual tests and are time consuming and require expensive equipment. In addition, often little differences are observed between fused images. Therefore evaluation criteria of the quality of different fused images have been proposed in recent years [12].

In statistical analysis, mean and standard deviation are defined as the following equations [13]:

$$\hat{\mu} = \frac{1}{MN}\sum_{i=1}^{M}\sum_{j=1}^{N} x_{i.j}$$

$$\hat{\sigma}^2 = \frac{1}{(M-1)(N-1)}\sum_{i=1}^{M}\sum_{j=1}^{N}(x_{i,j} - \hat{\mu})^2$$

Where MN is the pixel number in the image and xi,j is the value of ijth pixel.

Entropy is a measure of the information contained in the image. If the value of entropy is increased anter the fusion, the quality of the =information is increased. Entropy is mathematically defined as [13]:

$$E = -\sum_{i=1}^{M}\sum_{j=1}^{N} p(x_{ij}) \ln p(x_{ij})$$

where p(xij) is the probability of xij.

Off-centered entropy (OCE) is used to measure the differences of input and fused images. Lower values show that higher quality of the fused images.

$$OCE = (f_A, f_B : F) = \frac{CE(f_A, F) + CE(f_B, F)}{2}$$

Where fA and fB are input medical values from different modalities, F if fused image, $CE(f_A, F)\, CE(f_B, F)$ is off-centered entropy of original images $f_A(f_B)$ and F fused image.

$$CE(G, F) = \sum_{i=0}^{L-1} P_G(i) \log_2 \left|\frac{P_G(i)}{P_F(i)}\right|$$

$$G = A \; or \; B$$

Special frequency (SF) measures general activity level in an image. If SF value is increased after the fusion the activity is increased [13]. Mathematically:

$$Q_{i,j}^{F_1F} = Q_{g,i,j}^{F_1F} Q_{\alpha,i,j}^{F_1F} Q_{i,j}^{F_2F} = Q_{g,i,j}^{F_2F} Q_{\alpha,i,j}^{F_2F}$$

Where RF and CF are the raw and column frequencies which can be obtained by:

$$RF = \sqrt{\frac{1}{MN}\sum_{i=1}^{M_1}\sum_{j=2}^{N_1}[x_{i,j} - x_{i,j-1}]^2}$$

$$CF = \sqrt{\frac{1}{MN}\sum_{j=1}^{N_1}\sum_{i=2}^{M_1}[x_{i,j} - x_{i-1.j}]^2}$$

Mutual information (MI) is a measure of information which are common between the two images. If MI value is increased after the fusion, the quality of the information also increases [13]. Mathematically for MI we have:

$$MI = \sum_{i=1}^{l}\sum_{j=1}^{l} h_{i.j}^{x.y} \log_2 \frac{h_{i.j}^{x.y}}{h_{i,j}^{x} h_{i,j}^{y}}$$

where hxy is the histogram of gray level of x and y images, hx and hy are edge-normalized histograms for two images and L is the number of gray level. The more MI value is, the better the fused image becomes.

Structural similarities (SSIM) are expressed by modeling all types of image distortions as a combination of correlation loss, radio distortions and contrast distortions. SSIM is defined as equation (10-4):

$$SSIM = \frac{\sigma_{xy}}{\sigma_x \sigma_y} \frac{2\mu_x \mu_y}{\mu_x^2 + \mu_y^2} \frac{2\sigma_x \sigma_y}{\sigma_x^2 + \sigma_y^2}$$

Where μ_x and μ_y are intensity mean values and σ_x, σ_y and σ_{xy} are standard deviation. In the above equation the first term is correlation coefficient between x and y. The second term measures the proximity of gray level and the third term measures the contrast similarity between x and y. Higher SSIM values show better fusion of the image.

This criterion is indicative of the information contained in each input image which is transferred to the fused image. Mathematically $Q_s^{AB/F}$ is defined as equation (11-4) [14]:

$$Q_s^{F1F2/F} = \sum_{s \in S} c(s)(\lambda(s) SSIM(F1, F|s) + (1 - \lambda(s)) SSIM(F2, F|s))$$

where $(\lambda)S$ is significant information of F1 compared to F2 in driving window s and c(s) is the normalized window w. Its dynamic range is [-1, 1] and for better fusion it must be close to 1.

Similarity criterion based on edge investigates the converted edges in the fusion process and is mathematically defined as equation (12-4) [14]:

$$Q^{F_1F_2/F} = \frac{\sum_{i=1}^{M}\sum_{j=1}^{N}[Q_{i,j}^{F1F} w_{i,j}^{x} + Q_{i,j}^{F2F} w_{i,j}^{y}]}{\sum_{i=1}^{M}\sum_{j=1}^{N}[w_{i,j}^{x} + w_{i,j}^{y}]}$$

Where F1, F2 and F3 show the input and fused images. Definitions of Q^{F_1F} and Q^{F_2F} are similar:

Where Q_g^{*F} and Q_a^{*F} are edge intensity and the amount of

$$Q_{i,j}^{F_1F} = Q_{g,i,j}^{F_1F} Q_{\alpha,i,j}^{F_1F} Q_{i,j}^{F_2F} = Q_{g,i,j}^{F_2F} Q_{\alpha,i,j}^{F_2F}$$

direction preservation in (i, j) positions for F1 and F2 images. Dynamic range for $Q^{F_1F_2/F}$ is [0, 1] and for better fusion the value must be close to 1.

Correlation coefficient (cc) shows the small structures between the original and recovered values. Higher correlation indicates the preservation of more information [14].

$$cc(F,G) = \frac{\sum_{i=0}^{M-1}\sum_{j=0}^{N-1}(F(i,j)-\overline{F})(f_G(i,j)-\overline{f_G})}{\sqrt{\sum_{i=0}^{M-1}\sum_{j=0}^{N-1}(F(i,j)-\overline{F})^2 \sum_{i=0}^{M-1}\sum_{j=0}^{N-1}(f_G(i,j)-\overline{f_G})^2}}$$

$$G = A \; or \; B$$

For performance evaluation, the proposed image fusion strategy considered four groups of human brain images. In order to show superior performance of the proposed procedure, precise performance analysis was conducted by human brain images. These included MRI/SPECT and MRI/PET. All images were 256×256 in size. The images were downloaded from Harvard University website. It can be seen that due to different imaging principals and environments, reference image with different modalities had complementary information. For all these image groups, the results obtained from the proposed technique were compared by maximum values, mean values and counter let and violet based techniques. Visual comparison of the fused images is shown in figures 2, 3, 4 and 5. It is obvious that the proposed algorithm not only preserves the spectral information but also improves the information related to details of the location. Statistically, overall performance and comparison between the existing methods and the proposed algorithm are summarized in tables. In Figure 3, overall diagram of fusion is presented as a flowchart for the proposed algorithm.

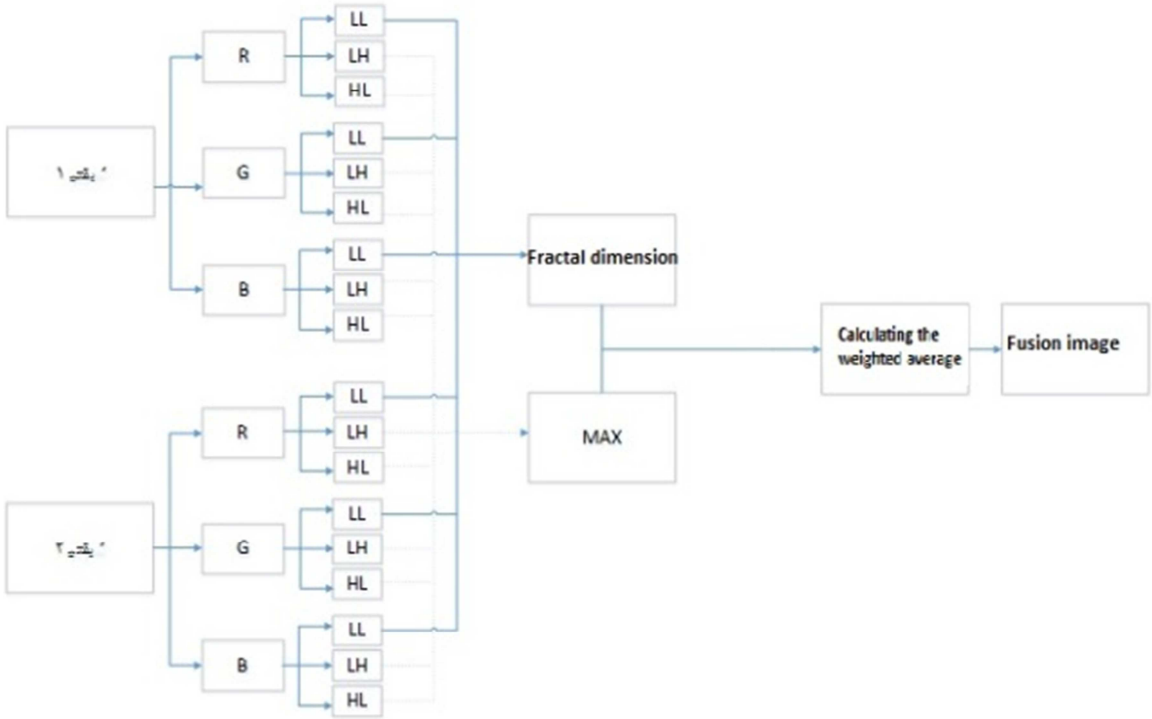

Figure 3. *Overall fusion diagram for the proposed technique.*

In the next section the analysis of 6 datasets is described. First in Figure 4 the analysis of the proposed algorithm for stroke patients is shown. Then, in Table 1, the evaluation indexes for the proposed algorithm along with previous algorithms for stroke patients are presented. In Figure 5 the analysis of the proposed algorithm for patients with Alzheimer's disease is presented. Then Table 2 summarizes the evaluation algorithm for the proposed algorithm along with previous algorithms for patients with Alzheimer's disease. Figure 6 shows the analysis of the proposed algorithm for patients with brain tumor. Then, in Table 3 the evaluation algorithm for the proposed algorithm along with previous algorithms for patients with brain tumor is summarized. In Figure 7 the analysis of the proposed algorithm for patients with head mass is presented. Then, Table 4 summarizes the evaluation algorithm for the proposed algorithm along with previous algorithms for patients with head masses. Figs. 8 and 9 show the proposed algorithm and finally Tables 5 and 6 present the information obtained from these images.

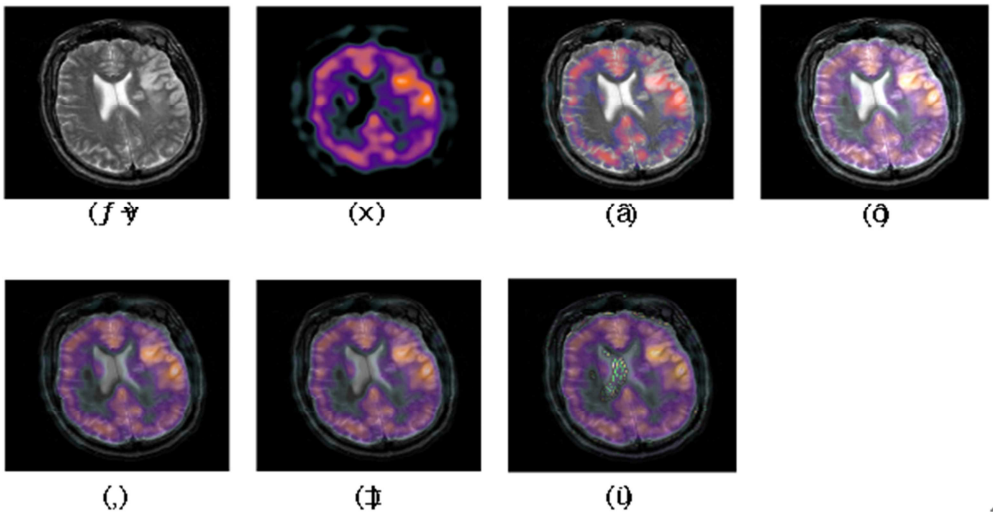

Figure 4. *Analysis of the proposed algorithm for stroke patients in a large region on the left side in brain vessels. a) original MRI image; b) original SPECT image; c) maximum; d) mean; e) violet; f) counterlet; g) image obtained by the proposed technique.*

Table 1. *evaluation index for fused image of Figure 4.*

	maximum	mean	wavelet	counterlet	Proposed technique
Mean	51.2681	60.4262	37.7209	37.6855	37.5949
SD	62.9698	74.6127	48.0505	47.9348	47.2309
Entropy	4.7961	5.1851	5.0977	5.1568	5.1728
SF	16.2757	17.95256	12.9309	12.5524	14.3875
SSIM1	0.98185	0.95256	0.96648	0.96839	0.9674
SSIM2	0.76354	0.69797	0.8853	0.88745	0.88107

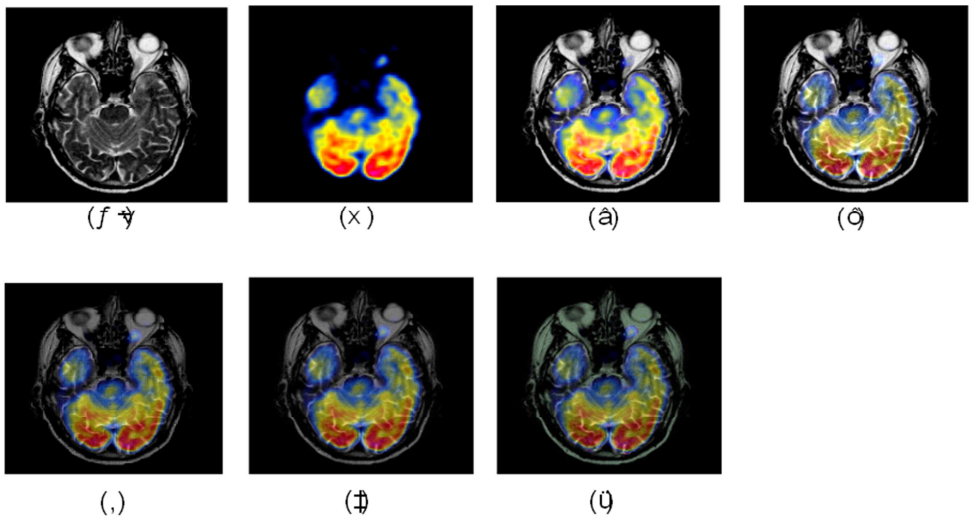

Figure 5. *Analysis of the proposed algorithm for patients with Alzheimer's disease. a) original MRI image; b) original PET image; c) maximum; d) mean; e) violet; f) counterlet; g) image obtained by the proposed technique.*

Table 2. *Evaluation index for fused image of Figure 5.*

	maximum	mean	wavelet	counter let	Proposed technique
Mean	49.8898	46.6652	30.0942	30.2167	30.3375
SD	77.5383	71.0493	48.1954	47.8457	46.4089
Entropy	3.8688	4.0183	3.9426	4.407	4.4202
SF	35.408	35.8426	24.859	25.6205	26.481
SSIM1	0.89227	0.91902	0.93435	0.94036	0.94847
SSIM2	0.62554	0.64592	0.79044	0.79004	0.77241

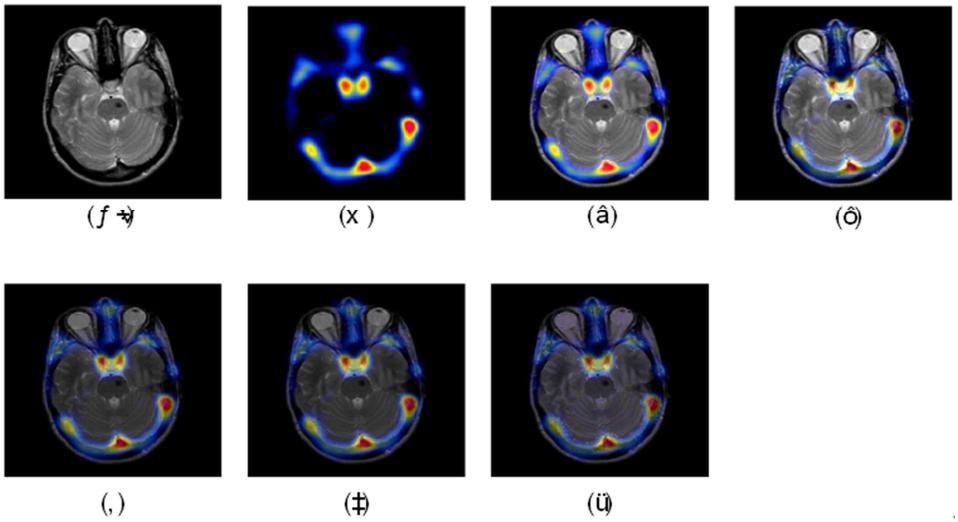

Figure 6. *Analysis of the proposed algorithm for patients with brain tumor. a) original MRI image; b) original PET image; c) maximum; d) mean; e) violet; f) counterlet; g) image obtained by the proposed technique.*

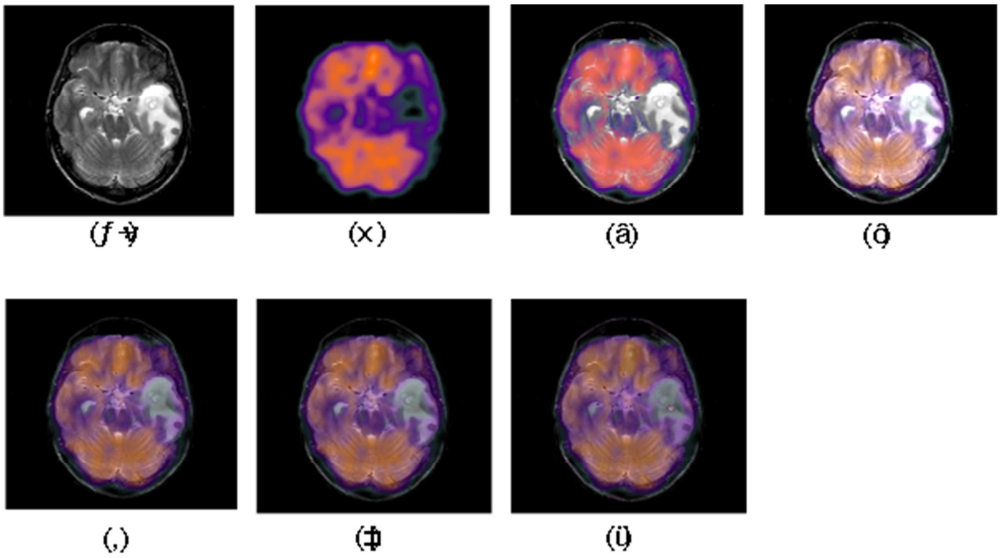

Figure 7. *Analysis of the proposed algorithm for patients with head mass. a) original MRI image; b) original SPECT image; c) maximum; d) mean; e) violet; f) counterlet; g) image obtained by the proposed technique.*

Table 3. *Evaluation index for fused image of Figure 6.*

	maximum	mean	wavelet	counterlet	Proposed technique
Mean	51.2681	60.4262	37.7209	37.6855	37.5949
SD	62.9698	74.6127	48.0505	47.9348	47.2309
Entropy	4.7961	5.1851	5.0977	5.1568	5.1728
SF	16.2757	17.95256	12.9309	12.5524	14.3875
SSIM1	0.98185	0.95256	0.96648	0.96839	0.9674
SSIM2	0.76354	0.69797	0.8853	0.88745	0.88107

Table 4. *Evaluation index for fused image of Figure 7.*

	maximum	mean	wavelet	counterlet	Proposed technique
Mean	50.7923	56.1114	37.8376	37.8503	37.1986
SD	71.5522	79.5888	53.4955	53.3476	51.82
Entropy	3.926	4.2703	4.1592	4.3711	4.3594
SF	14.9686	17.6084	12.8329	12.1132	12.3335
SSIM1	0.91316	0.90192	0.96252	0.96406	0.96591
SSIM2	0.90849	0.86455	0.94297	0.94395	0.94141

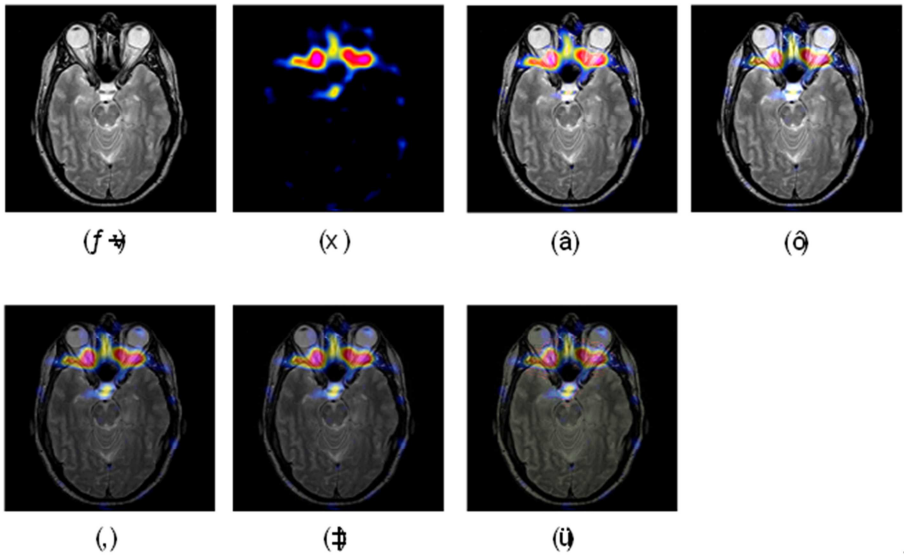

Figure 8. *Analysis of the proposed algorithm. a) original MRI image; b) original PET image; c) maximum; d) mean; e) violet; f) counterlet; g) image obtained by the proposed technique.*

Table 5. *Evaluation index for fused image of Figure 8.*

	maximum	**mean**	**wavelet**	**counterlet**	**Proposed technique**
Mean	53.7741	53.5117	29.2454	29.2761	30.7415
SD	67.9909	68.0647	40.1981	39.9298	40.4644
Entropy	3.8971	4.027	4.3531	4.6675	4.7009
SF	25.6933	25.8287	18.759	18.4864	19.3643
SSIM1	0.97692	0.98078	0.86351	0.86749	0.88339
SSIM2	0.15547	0.15444	0.28453	0.2843	0.26745

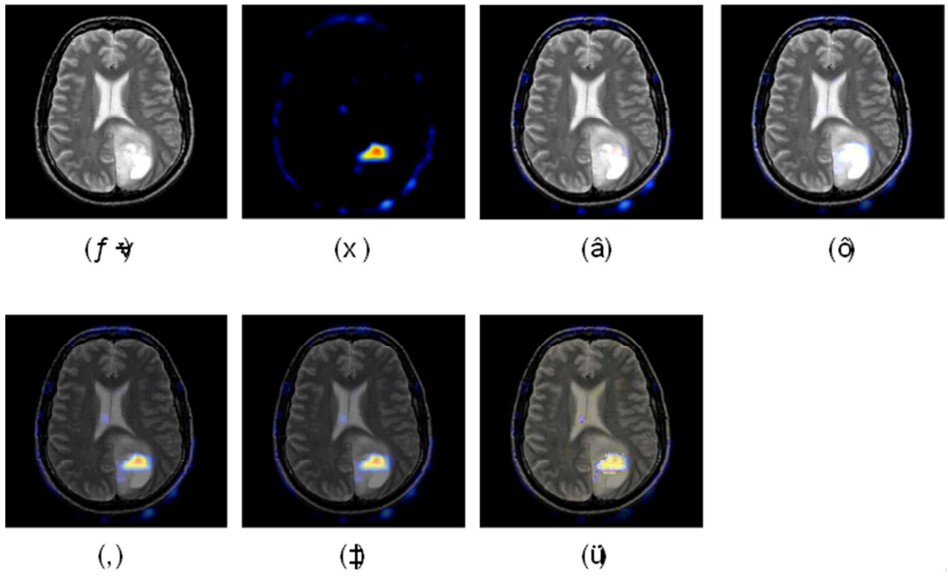

Figure 9. *Analysis of the proposed algorithm. a) original MRI image; b) original PET image; c) maximum; d) mean; e) violet; f) counterlet; g) image obtained by the proposed technique.*

Table 6. *Evaluation index for fused image of Figure 7.*

	maximum	**mean**	**wavelet**	**counterlet**	**Proposed technique**
Mean	54.0437	53.9756	28.2457	28.2788	37.1266
SD	68.3771	68.9213	37.6996	37.4165	46.7475
Entropy	3.8039	3.8776	4.2597	4.5751	4.7891
SF	22.9587	23.1193	15.9137	15.1629	17.9073
SSIM1	0.98594	0.98999	0.82991	0.83407	0.93173
SSIM2	0.05202	0.05075	0.10395	0.10405	0.07524

In the above comparisons it was observed that among the results obtained from 6 datasets the proposed algorithms had better performance. For comparison, 5 factors were used in each 6 dataset. In investigating all factors of the proposed algorithm, better performance was observed. This proved that image fusion by the proposed method in medical domain provided better responses.

4. Conclusion

In order to prove excellent performance of the proposed technique, a precise performance analysis was conducted using brain images. In these images, brain tumors, Alzheimer disease and stroke were investigated using MRI/PET and MRI/SPECT images. For image fusion, counterlet transformation was conducted on MRI, PET and SPECT images in RGB mode. Here, the obtained results were compared with images obtained by different other techniques. Generally, the results obtained from the proposed method had very smaller mean and standard deviation compared to counterlet and wavelet techniques. The proposed method outperformed counterlet and wavelet techniques in terms of entropy criterion. Regarding structural similarity, the proposed method showed better performance in terms of maximum and mean values and had very small differences with wavelet and counterlet techniques.

References

[1] G. Dougherty, Digital image processing for medical applications: Cambridge University Press, 2009.

[2] C. He, Q. Liu, H. Li, and H. Wang, "Multimodal medical image fusion based on IHS and PCA," Procedia Engineering, vol. 7, pp. 280-285, 2010.

[3] Z. Xu, "Medical image fusion using multi-level local extrema," Information Fusion, vol. 19, pp. 38-48, 2014.

[4] S. R. Cherry, J. A. Sorenson, and M. E. Phelps, Physics in nuclear medicine: Elsevier Health Sciences, 2012.

[5] A. Webb and G. C. Kagadis, Introduction to biomedical imaging: Wiley Hoboken, 2003.

[6] T. Stathaki, Image fusion: algorithms and applications: Academic Press, 2011.

[7] S. Zheng, "Pixel-level Image Fusion Algorithms for Multi-camera Imaging System," 2010.

[8] D. K. Sahu and M. Parsai, "Different image fusion techniques–a critical review," International Journal of Modern Engineering Research (IJMER), vol. 2, pp. 4298-4301, 2012.

[9] K. G. Baum, M. Helguera, and A. Krol, "Fusion viewer: a new tool for fusion and visualization of multimodal medical data sets," Journal of Digital Imaging, vol. 21, pp. 59-68, 2008.

[10] M. Aguilar and A. L. Garrett, "Neurophysiologically-motivated sensor fusion for visualization and characterization of medical imagery," in Proc. of the Fourth International Conference on Information Fusion, 2001.

[11] http://www.med.harvard.edu/aanlib/sponsor.html, harvard.

[12] Z. Wang, D. Ziou, C. Armenakis, D. Li, and Q. Li, "A comparative analysis of image fusion methods," Geoscience and Remote Sensing, IEEE Transactions on, vol. 43, pp. 1391-1402, 2005.

[13] G. Bhatnagar, Q. J. Wu, and Z. Liu, "Human visual system inspired multi-modal medical image fusion framework," Expert Systems with Applications, vol. 40, pp. 1708-1720, 2013.

[14] G. Piella and H. Heijmans, "A new quality metric for image fusion," in Image Processing, 2003. ICIP 2003. Proceedings. 2003 International Conference on, 2003, pp. III-173-6 vol. 2.